

EXTREME EVENT QUANTIFICATION IN DYNAMICAL SYSTEMS WITH RANDOM COMPONENTS

GIOVANNI DEMATTEIS, TOBIAS GRAFKE, AND ERIC VANDEN-EIJNDEN

ABSTRACT. A central problem in uncertainty quantification is how to characterize the impact that our incomplete knowledge about models has on the predictions we make from them. This question naturally lends itself to a probabilistic formulation, by making the unknown model parameters random with given statistics. Here this approach is used in concert with tools from large deviation theory (LDT) and optimal control to estimate the probability that some observables in a dynamical system go above a large threshold after some time, given the prior statistical information about the system's parameters and/or its initial conditions. Specifically, it is established under which conditions such extreme events occur in a predictable way, as the minimizer of the LDT action functional. It is also shown how this minimization can be numerically performed in an efficient way using tools from optimal control. These findings are illustrated on the examples of a rod with random elasticity pulled by a time-dependent force, and the nonlinear Schrödinger equation (NLSE) with random initial conditions.

1. INTRODUCTION

The governing equations we use to model complex phenomena are often approximate. For example, we may not know exactly the initial and/or boundary conditions necessary to integrate these equations. Other parameters entering these equations can also be uncertain, either because we are not sure of the model itself or because these parameters may vary from situations to situations in a way that is difficult to predict in detail. The question then becomes whether we can quantify how our imperfect knowledge of the system's parameters impact its behavior. This question lends itself naturally to a probabilistic formulation. Consider for example the case of a dynamical system whose state at time t can be specified by some $u(t)$ which can be a vector or a field and satisfies

$$\partial_t u = b(u, \vartheta), \quad u(t=0) = u_0(\vartheta). \quad (1)$$

Here $b(u, \vartheta)$ is a given vector field and ϑ denotes the set of parameters we are uncertain of. Assuming that these parameters take value in some set Ω , which can again be finite or infinite dimensional, it is then natural to equip Ω with a probability measure μ to quantify our uncertainty. This makes ϑ random, and therefore the solution to (1) becomes a stochastic process. Denoting it by $u(\cdot, \vartheta)$, we can ask questions about the statistics of this process. For example, if $f(u)$ is a scalar valued observable, we can define

$$P_T(z) \equiv \mathbb{P}(f(u(T, \vartheta)) \geq z), \quad z \in \mathbb{R}, \quad (2)$$

where \mathbb{P} denotes the probability over μ and $T > 0$ is some observation time. The probability (2) is useful e.g. in the context of certification problem where, given $z \in \mathbb{R}$ and $\epsilon > 0$ (typically z large and ϵ small), we wish to verify that $P_T(z) \leq \epsilon$. Other quantities of interest include

$$\mathbb{P}\left(\int_0^T f(u(t, \vartheta)) dt \geq z\right), \quad \mathbb{P}\left(\sup_{0 \leq t \leq T} f(u(t, \vartheta)) \geq z\right), \quad \text{etc.} \quad (3)$$

The numerical estimation of (2) or (3) can be performed by Monte Carlo sampling methods: generate N independent realizations of ϑ , for each evaluate $f(u(T, \vartheta))$ via integration of (1), and compute the fraction of these realizations for which $f(u(T, \vartheta)) \geq z$. As $N \rightarrow \infty$, this fraction will

converge to $P_T(z)$. This direct approach is not effective when $P_T(z)$ is small, however, since the relative error of the estimator just described is $\sqrt{(1 - P_T(z))/(NP_T(z))} \sim 1/\sqrt{NP_T(z)}$. This means that in order to get an estimate accurate to order $\delta \ll 1$, we need to use $N = O(\delta^{-2} P_T^{-1}(z))$ samples, which can become prohibitively expensive as $P_T(z)$ gets smaller. This is problematic since it excludes from consideration events that are rare but may nonetheless have dramatic consequences. Similar issues arise if we replace (1) by some time independent equation like

$$0 = b(u, \vartheta), \quad (4)$$

where $b(\cdot, \vartheta)$ is some function of u and possibly its derivatives and (4) is supplemented with boundary conditions that may also depend on the random parameter ϑ . The solution to (4) defines a complicated map $u(\vartheta)$, and given a scalar valued observable $f(u)$, the estimation of

$$\mathbb{P}(f(u(\vartheta)) \geq z), \quad z \in \mathbb{R} \quad (5)$$

will again be challenging when this probability is small, i.e. when the event $f(u(\vartheta)) \geq z$ is rare.

In these situations alternative methods such as those proposed e.g. in [9, 17, 19, 20, 26, 35, 38, 41] must be used to estimate (2), (3), or (5). The approach we introduce in this paper builds on earlier results found in [13] and uses large deviation theory (LDT) [14, 42] as a tool: we show that, if in (2) $P_T(z) \rightarrow 0$ as $z \rightarrow \infty$, then under some additional assumptions we have

$$P_T(z) \asymp \exp\left(-\min_{\theta \in \Omega(z)} I(\theta)\right) \quad \text{where} \quad \Omega(z) = \{\theta : f(u(T, \theta)) \geq z\} \subseteq \Omega. \quad (6)$$

Here \asymp indicates that the ratio of logarithms of both sides tends to 1 as $z \rightarrow \infty$ and we defined

$$I(\theta) = \max_{\eta} (\langle \eta, \theta \rangle - S(\eta)), \quad (7)$$

where $\langle \cdot, \cdot \rangle$ is a suitable inner product on Ω and $S(\eta)$ is the cumulant generating function of ϑ :

$$S(\eta) = \log \mathbb{E} e^{\langle \eta, \vartheta \rangle} = \log \int_{\Omega} e^{\langle \eta, \theta \rangle} d\mu(\theta). \quad (8)$$

We will also show that the minimizer of $I(\theta)$ in $\Omega(z)$, i.e.

$$\theta^*(z) = \operatorname{argmin}_{\theta \in \Omega(z)} I(\theta), \quad (9)$$

is the point of maximum likelihood in $\Omega(z)$. The most likely way the event $\{f(u(T, \vartheta)) \geq z\}$ occurs is when $\vartheta = \theta^*(z)$. Similar estimates hold for (3) and (5) upon straightforward redefinition of the set $\Omega(z)$ upon which the optimization is performed.

Establishing the large deviation principle (LDP) in (6) is one of the objectives of this paper. As we will see in Sec. 2, this can be done by proving that $\theta^*(z)$ is a dominating point in $\Omega(z)$, building on results derived e.g. in [5, 7, 24, 31] that provide us with a framework to justify the saddle-point approximations often used in physics [18, 25]. Eq. (6) is a somewhat unusual LDP however because there is no small (or large) parameter associated to the random variable ϑ : rather we play with the variable z being large. More precisely, instead of scaling ϑ so that events with a finite z become rare, we keep ϑ as is and look at rare events that occur in the tail of the distribution when $z \gg 1$. As a result, the standard approach developed in [5, 24, 31] must be adapted. Of course, both viewpoints are equivalent up to some appropriate rescaling of the variables ϑ and z , but this rescaling involves the so-called speed of the LDP, which is unknown to us *a priori*. The formulation we adopt can be viewed as a way to estimate this speed.

When (6) holds, we can reduce the evaluation of $P_T(z)$ to the minimization problem in (9), and a second objective here is to design numerical tools to perform this minimization. As we will see in Sec. 3, this can be done by adapting techniques used in optimal control [6, 40].

We will also illustrate these tools on two examples in Sec. 4: The first one is a model for an elastic rod with a random elasticity coefficient. The rod gets pulled from one end with a given forcing protocol, and the response depends nonlinearly on the elasticity coefficient. The LDP can be used here to infer the probability of atypically large extensions of the rod. The second

application deals with the nonlinear Schrödinger equation (NLSE) in nonlinear fiber optics, in the context of what is known as integrable turbulence, and study the problem of the onset of rogue waves out of a bath of random waves taken as initial condition for NLSE.

2. LARGE DEVIATION PRINCIPLE

Here we establish (6), using background material that can be e.g. found in [5, 24, 31]. For simplicity, we will restrict ourselves to situations where ϑ is finite dimensional, i.e. we assume that $\vartheta \in \Omega \subseteq \mathbb{R}^M$ with $M \in \mathbb{N}$. In this case we can also assume that the inner product $\langle \cdot, \cdot \rangle$ appearing in (7) and (8) is the standard Euclidean inner product on \mathbb{R}^M . Under appropriate assumptions, the results below will hold also in the infinite-dimensional set-up, when ϑ is a random field, but the arguments to establish them will require generalization (see e.g. [15, 29] for results in infinite dimension). To treat the problems in (2), (3) and (5) on the same footing we also define the map $F : \Omega \rightarrow \mathbb{R}$ via

$$F(\theta) = f(u(T, \theta)), \quad \text{for (2)}$$

$$F(\theta) = \int_0^T f(u(T, \theta)) dt, \quad \text{or} \quad F(\theta) = \sup_{0 \leq t \leq T} f(u(t, \theta)), \quad \text{for (3)} \quad (10)$$

$$F(\theta) = f(u(\theta)) \quad \text{for (5)}$$

so that we can recast these probabilities into

$$P(z) = \mathbb{P}(F(\vartheta) \geq z) = \mu(\Omega(z)) \quad \text{where} \quad \Omega(z) = \{\theta : F(\theta) \geq z\}. \quad (11)$$

To proceed, we start by making two assumptions:

Assumption 1. *The map F is continuously differentiable, and such that $|\nabla F(\theta)| \geq K > 0$ for all $\theta \in \Omega$.*

Assumption 2. *The measure μ is such that (this is (8))*

$$S(\eta) = \log \mathbb{E} e^{\langle \eta, \vartheta \rangle} = \log \int_{\Omega} e^{\langle \eta, \theta \rangle} d\mu(\theta) \quad (12)$$

exists for all $\eta \in \mathbb{R}^M$ and defines a differentiable function $S : \mathbb{R}^M \rightarrow \mathbb{R}$.

Ultimately, Assumption 1 is about the specifics of the governing equation in (1) or (4) and the observable f : since the field u is typically a complicated function of ϑ , establishing the conditions under which this assumption holds will have to be done on a case-by-case basis. Note that it guarantees that the set $\Omega(z)$ is simply connected with a boundary that is C^1 for all $z \in \mathbb{R}$, with inward pointing unit normal at $\theta(z) \in \partial\Omega(z)$ given by $\hat{n}(z) = \nabla F(\theta(z)) / |\nabla F(\theta(z))|$. We could relax the constraint $|\nabla F(\theta)| > 0$, and allow e.g. for the sets $\Omega(z)$ to have several connected components (the number of which could depend on z), but this requires to modify the argument below. Assumption 2 allows us to introduce the tilted measure

$$d\mu_{\eta}(\theta) = \frac{e^{\langle \eta, \theta \rangle} d\mu(\theta)}{\int_{\Omega} e^{\langle \eta, \theta \rangle} d\mu(\theta)} = e^{\langle \eta, \theta \rangle - S(\eta)} d\mu(\theta). \quad (13)$$

It is easy to see that the mean of μ_{η} is shifted compared to that of μ . A simple calculation shows that

$$\int_{\Omega} \theta d\mu_{\eta}(\theta) = \nabla S(\eta), \quad (14)$$

and this will allow us to pick η such that the mean of μ_{η} is precisely at the point minimizing $I(\theta)$ in $\Omega(z)$. Note that

$$\Omega(z + \delta) \subseteq \Omega(z) \quad \forall z \in \mathbb{R}, \delta \geq 0, \quad (15)$$

and to establish (6) we will find conditions such that (i) $\mu(\Omega(z))$ decreases fast with z and (ii) this probability is dominated by a small region around a single point on $\partial\Omega(z)$. This will require us to make additional assumptions on the geometry of $\Omega(z)$ that we discuss next in connection with properties of the rate function $I(\theta)$ defined in (7).

Letting

$$\theta^*(z) = \operatorname{argmin}_{\theta \in \Omega(z)} I(\theta), \quad (16)$$

we first make:

Assumption 3. *There exists a finite z_0 such that, $\forall z \geq z_0$, $\theta^* : [z_0, \infty) \rightarrow \Omega$ is continuously differentiable and $I(\theta^*(\cdot))$ is strictly increasing with z with*

$$I(\theta^*(z)) \rightarrow \infty \quad \text{and} \quad |\nabla I(\theta^*(z))| \geq K > 0 \quad \text{as} \quad z \rightarrow \infty. \quad (17)$$

This assumption implies that $\theta^*(z) \in \partial\Omega(z)$ for $z > z_0$, i.e. we can replace (16) with

$$\theta^*(z) = \operatorname{argmin}_{\theta \in \partial\Omega(z)} I(\theta). \quad (18)$$

The Euler Lagrange equation for (18) is

$$\nabla I(\theta^*(z)) = \lambda \nabla F(\theta^*(z)) \quad (19)$$

for some Lagrange multiplier λ . Since by definition both S and I are convex functions, by the involution property of the Legendre transform we have

$$S(\eta) = \max_{\theta} (\langle \eta, \theta \rangle - I(\theta)), \quad (20)$$

and this maximum is achieved at the solution of

$$\eta = \nabla I(\theta) \quad (21)$$

in θ . Therefore if we define $\eta^*(z)$ via

$$\eta^*(z) = \nabla I(\theta^*(z)) \quad (22)$$

the mean of $\mu_{\eta^*(z)}$ is $\theta^*(z)$. From (20) this also implies that

$$\langle \eta^*(z), \theta^*(z) \rangle - S(\eta^*(z)) = I(\theta^*(z)), \quad (23)$$

which gives the following exact representation formula for $\mu(\Omega(z))$

$$\begin{aligned} \mu(\Omega(z)) &= \int_{\Omega(z)} e^{S(\eta^*(z)) - \langle \eta^*(z), \theta \rangle} d\mu_{\eta^*(z)}(\theta) \\ &= e^{-I(\theta^*(z))} \int_{\Omega(z)} e^{-\langle \eta^*(z), \theta - \theta^*(z) \rangle} d\mu_{\eta^*(z)}(\theta). \end{aligned} \quad (24)$$

To proceed further we need to make some assumptions about $\Omega(z)$. First:

Assumption 4. *For all $z \geq z_0$, the set $\Omega(z)$ is contained in the half-space whose boundary is tangent to $\Omega(z)$ at $\theta = \theta^*(z)$, i.e.*

$$\Omega(z) \subseteq \mathcal{H}(z) = \{\theta : \langle \hat{n}^*(z), \theta - \theta^*(z) \rangle \geq 0\}, \quad (25)$$

where $\hat{n}^*(z) = \nabla F(\theta^*(z)) / |\nabla F(\theta^*(z))|$ denotes the inward pointing unit normal to $\partial\Omega(z)$ at $\theta^*(z)$.

In the terminology of Ney [31], it means that $\theta^*(z)$ is a dominating point in $\Omega(z)$. If we combine (19) and (22) we deduce that

$$\frac{\eta^*(z)}{|\eta^*(z)|} = \frac{\nabla F(\theta^*(z))}{|\nabla F(\theta^*(z))|} = \hat{n}^*(z) \quad (26)$$

and as a result we can use Fubini's theorem to express (24) as

$$\mu(\Omega(z)) = e^{-I(\theta^*(z))} \int_0^\infty e^{-|\eta^*(z)|s} |\eta^*(z)| G(z, s) ds. \quad (27)$$

Here we defined

$$G(z, s) = \mu_{\eta^*(z)}(\Omega(z) \setminus \mathcal{H}(z, s)), \quad (28)$$

with

$$\mathcal{H}(z, s) = \{\theta : \langle \hat{n}^*(z), (\theta - \theta^*(z) - \hat{n}^*(z)s) \rangle \geq 0\}. \quad (29)$$

Note that in (27) the lower limit of the integral is at $s = 0$ by Assumption 4. Since by definition we have

$$\forall s > 0 : G(z, s) \in (0, 1), \quad \forall s, s' > 0, s' > s : G(z, s') > G(z, s), \quad \lim_{s \rightarrow 0^+} G(z, s) = 0, \quad (30)$$

from (27) we obtain the upper bound

$$\mu(\Omega(z)) \leq e^{-I(\theta^*(z))} \int_0^\infty e^{-|\eta^*(z)|s} |\eta^*(z)| ds = e^{-I(\theta^*(z))}, \quad (31)$$

which implies

$$\frac{\log \mu(\Omega(z))}{I(\theta^*(z))} \leq -1. \quad (32)$$

To get a matching lower bound notice that for all $s_1 > 0$ we have

$$\begin{aligned} \mu(\Omega(z)) &\geq e^{-I(\theta^*(z))} \int_0^{s_1} e^{-|\eta^*(z)|s} |\eta^*(z)| G(z, s) ds \\ &\geq e^{-I(\theta^*(z))} G(z, s_1) \left(1 - e^{-|\eta^*(z)|s_1}\right) \\ &\geq e^{-I(\theta^*(z))} G(z, s_1) \frac{|\eta^*(z)|s_1}{1 + |\eta^*(z)|s_1}. \end{aligned} \quad (33)$$

Therefore if we make:

Assumption 5. *There exists $s_1 > 0$ such that*

$$\lim_{z \rightarrow \infty} \frac{\log G(z, s_1)}{I(\theta^*(z))} = 0, \quad (34)$$

for this s_1 we have (using also Assumption 3 that guarantees that $|\eta^*(z)| \geq K > 0$)

$$\begin{aligned} \frac{\log \mu(\Omega(z))}{I(\theta^*(z))} &\geq -1 + \frac{\log G(z, s_1) + \log(|\eta^*(z)|s_1) - \log(1 + |\eta^*(z)|s_1)}{I(\theta^*(z))} \\ &= -1 + \frac{\log G(z, s_1) - \log(1 + |\eta^*(z)|^{-1}s_1^{-1})}{I(\theta^*(z))} \\ &\rightarrow -1 \quad \text{as } z \rightarrow \infty. \end{aligned} \quad (35)$$

Combining (32) and (35) we finally deduce

Theorem 1 (Large deviation principle). *Under Assumptions 1–5, the following result holds:*

$$\lim_{z \rightarrow \infty} \frac{\log P(z)}{I(\theta^*(z))} = \lim_{z \rightarrow \infty} \frac{\log \mu(\Omega(z))}{I(\theta^*(z))} = -1. \quad (36)$$

Note that (36) is just a rephrasing of (6).

It is useful to comment on the assumptions on $\Omega(z)$ that lead to Theorem 1. Assumption 3 states that the event $\{F(\theta) \geq z\}$ becomes rare as $z \rightarrow \infty$, which is clearly necessary for an LDP to apply. Assumption 4 guarantees that all regions in $\Omega(z)$ remain much more unlikely than $\theta^*(z)$: this assumption can be relaxed, but at the price of having to analyze more carefully how $I(\theta)$ behaves on $\partial\Omega(z)$ and exclude that regions with lower likelihood near this boundary accumulate and eventually dominate the probability. Finally, Assumption 5 is about the shape of the set $\Omega(z)$ near $\theta^*(z)$. Since the mean of $\mu_{\eta^*(z)}$ is $\theta^*(z)$, we know that this measure must have mass in a region around $\theta^*(z)$ but we need to make sure that this region has sufficient overlap with $\Omega(z)$. For example, if for each $z \geq z_0$ we can insert in $\Omega(z)$ a set that contains $\theta^*(z)$ on its boundary and is such that its volume remains finite as $z \rightarrow \infty$, Assumption 5 will automatically hold. On the other hand, this assumption could fail for example if $\Omega(z)$ becomes increasingly thin. More discussion about this kind of geometric assumptions can be found e.g. in [23, 29].

It is also interesting to note that (27) offers a way to derive asymptotic expansions for $\mu(\Omega(z))$ more refined than (36) if we assume that: (i) $|\eta^*(z)|$ grows with z , i.e. we supplement (17) with

$$|\eta^*(z)| = |\nabla I(\theta^*(z))| \rightarrow \infty \quad \text{as } z \rightarrow \infty; \quad (37)$$

and (ii) $G(z, s)$ has a specific behavior near $s = 0$ as $z \rightarrow \infty$. For example, suppose that there is a $C > 0$ such that for all $u \geq 0$

$$G(z, |\eta^*(z)|^{-1}u) \sim C|\eta^*(z)|^{-\alpha}u^\alpha \quad \text{with } \alpha > 0 \text{ as } z, |\eta^*(z)| \rightarrow \infty, \quad (38)$$

where $f(z) \sim g(z)$ indicates that $\lim_{z \rightarrow \infty} f(z)/g(z) = 1$. Then we have

$$\begin{aligned} P(z) = \mu(\Omega(z)) &= e^{-I(\theta^*(z))} \int_0^\infty e^{-u} G(z, |\eta^*(z)|^{-1}u) du \\ &\sim e^{-I(\theta^*(z))} C|\eta^*(z)|^{-\alpha} \int_0^\infty e^{-u} u^\alpha du \\ &= C\Gamma(\alpha+1)|\eta^*(z)|^{-\alpha} e^{-I(\theta^*(z))}. \end{aligned} \quad (39)$$

It is interesting to note that both (27) and (39) are consistent with $\vartheta|_{\Omega(z)}$ (outcome of the event conditioned on $F(\vartheta) \geq z$) having fluctuations of order $O(|\eta^*(z)|^{-1})$ away from $\theta^*(z)$ in the direction parallel to $\eta^*(z)$. Perpendicular to $\eta^*(z)$ the fluctuations remain of order $O(1)$ even as $z \rightarrow \infty$, but integrating in these perpendicular directions only gives a sub-exponential correction to $\mu(\Omega(z))$. This correction depends on the geometry of the hypersurface $\partial\Omega(z)$ (in particular on its curvature) near $\theta^*(z)$. This is what is accounted for in (39), and this picture will be confirmed in the numerical examples below.

Illustration: Gaussian measure with linear observable. Let us illustrate the LDT optimization in the simple case of a Gaussian random variable ϑ with mean 0 and covariance Id, taking values $\theta \in \mathbb{R}^N$. If we consider a linear observable

$$F(\theta) = \langle b, \theta \rangle, \quad b \in \mathbb{R}^N, \quad (40)$$

we have

$$\mathbb{P}(\langle b, \vartheta \rangle \geq z) = (2\pi)^{-N/2} \int_{\langle b, \theta \rangle \geq z} \exp\left(-\frac{1}{2}|\theta|^2\right) d\theta, \quad (41)$$

and a direct calculation shows that

$$\mathbb{P}(\langle b, \vartheta \rangle \geq z) = \frac{1}{2} \operatorname{erfc}\left(\frac{z}{\sqrt{2}|b|}\right) \sim (2\pi)^{-1/2} |b| z^{-1} \exp\left(-\frac{1}{2}|b|^{-2} z^2\right) \quad \text{as } z \rightarrow \infty. \quad (42)$$

Let us check that the LDP derived above is consistent with this result. Here

$$I(\theta) = \frac{1}{2}|\theta|^2, \quad S(\eta) = \frac{1}{2}|\eta|^2. \quad (43)$$

If we minimize $I(\theta)$ subject to $\langle \theta, b \rangle \geq z$, we deduce

$$\theta^*(z) = z|b|^{-2}b \quad \text{and} \quad I(\theta^*(z)) = \frac{1}{2}|b|^{-2}z^2. \quad (44)$$

Comparing this result with (42) we see that it is consistent with the prediction in (36).

We can also test what the theory can say beyond the log-asymptotic estimate. Here, the planar condition corresponding to $\Omega(z) = \mathcal{H}(z)$ is exactly fulfilled by linearity of $F(\theta) = \langle b, \theta \rangle$. We need to estimate $G(z, |\eta^*(z)|^{-1})$ as $z \rightarrow \infty$. From (22) and (23) we have that

$$\eta^*(z) = \nabla I(\theta^*(z)) = \theta^*(z) = z|b|^{-2}b, \quad S(\eta^*(z)) = \frac{1}{2}z^2|b|^{-2}, \quad (45)$$

and the tilted measure (13) at $\eta = \eta^*(z)$ reads

$$d\mu_{\eta^*(z)}(\theta) = (2\pi)^{-N/2} \exp\left(-\frac{1}{2}|\theta|^2 + z|b|^{-2}\langle b, \theta \rangle - \frac{1}{2}z^2|b|^{-2}\right) d\theta. \quad (46)$$

Using (45), we obtain

$$\begin{aligned} G(z, s) &= \int_{z \leq \langle b, \theta \rangle \leq z+s} d\mu_{\eta^*(z)}(\theta) \\ &= (2\pi)^{-1/2} \int_0^s \exp\left(-\frac{1}{2}u^2\right) du \\ &= \frac{1}{2} \operatorname{erf}\left(\frac{1}{2}\sqrt{2}s\right). \end{aligned} \quad (47)$$

As a result

$$G(z, |\eta^*(z)|^{-1}s) \sim (2\pi)^{-1/2} |\eta^*(z)|^{-1}s = (2\pi)^{-1/2} |b| s z^{-1} \quad \text{as } z \rightarrow \infty. \quad (48)$$

Comparing with (38), we see that here $C = (2\pi)^{-1/2}$ and $\alpha = 1$. Therefore (39) agrees with (42) as expected.

3. NUMERICAL ASPECTS

Here we review how to numerically perform the minimization in (6) and thereby estimate $P(z)$ – the method can be straightforwardly generalized to consider also the minimization associated with the calculation of (3) or (5). We impose the constraint $f(u(T)) \geq z$ by adding a Lagrange multiplier term to (6), so that the minimization can be rephrased in Hamiltonian formalism by [6, 40]:

$$E(u, \theta) = I(\theta) - \lambda f(u(T)), \quad (49)$$

where $u(T)$ should itself be viewed as a function of θ obtained by solving (1) with $\vartheta = \theta$, that is

$$\partial_t u = b(u, \theta), \quad u(t=0) = u_0(\theta). \quad (50)$$

The minimization of (49) with $u(T)$ obtained from (50) can be performed via steepest descent with adaptive step (line search). This requires to compute the gradient of E with respect to θ , which can be achieved in two ways: by the direct and the adjoint methods [6, 34]. These steps are described next.

3.1. Gradient Calculation.

3.1.1. *Direct method.* The gradient of the cost function with respect to the control reads:

$$\nabla_\theta E(u(T, \theta), \theta) = \partial_\theta E + (\partial_\theta u(T, \theta))^T \partial_u E = \nabla_\theta I - \lambda J^T(T, \theta) \partial_u f(u(T, \theta)), \quad (51)$$

where $J = \partial_\theta u$ is the Jacobian—componentwise $J_{i,j} = \partial u_i / \partial \theta_j$. An evolution equation for J can be obtained by differentiating (50) with respect to θ :

$$\partial_t J = \partial_u b J + \partial_\theta b, \quad J(0) = \nabla_\theta u_0. \quad (52)$$

Summing up, given the current state of the control, θ^n , we calculate the gradient of the objective function via:

- (1) *Field estimation:* Obtain the current field u^n by solving

$$\partial_t u^n = b(u^n, \theta^n), \quad u^n(0) = u_0(\theta^n). \quad (53)$$

- (2) *Jacobian estimation:* Obtain the Jacobian J^n by solving

$$\partial_t J^n = \partial_u b(u^n, \theta^n) J^n + \partial_\theta b(u^n, \theta^n), \quad J^n(0) = \nabla_\theta u_0(\theta^n). \quad (54)$$

- (3) *Gradient calculation:* Compute the gradient $(\nabla_\theta E)^n$ via

$$(\nabla_\theta E)^n = \nabla_\theta I(\theta^n) - \lambda (J^n(T))^T \partial_u f(u^n(T)). \quad (55)$$

3.1.2. *Adjoint method.* Let us introduce the adjoint field $\mu(t)$ solution of

$$\partial_t \mu = -(\partial_u b)^T \mu, \quad \mu(T, \theta) = \lambda \partial_u f(u(T, \theta)). \quad (56)$$

Using this equation as well as the transpose of (52) we deduce

$$\begin{aligned} \partial_t (J^T \mu) &= \partial_t J^T \mu + J^T \partial_t \mu \\ &= J^T (\partial_u b)^T \mu + (\partial_\theta b)^T \mu - J^T (\partial_u b)^T \mu = (\partial_\theta b)^T \mu. \end{aligned} \quad (57)$$

As a result

$$\int_0^T (\partial_\theta b)^T \mu dt = J^T(T) \mu(T) - J^T(0) \mu(0) = \lambda J^T(T, \theta) \partial_u f(u(T, \theta)) - (\nabla_\theta u_0)^T \mu(0, \theta). \quad (58)$$

This expression offers a way to write the gradient of the objective function in (51) as

$$\nabla_{\theta} E = \nabla_{\theta} I - (\nabla_{\theta} u_0)^T \mu(0, \theta) - \int_0^T (\partial_{\theta} b)^T \mu dt. \quad (59)$$

Using this expression instead of (51) is computationally advantageous because it avoids the calculation of the Jacobian J – note in particular that the adjoint field μ has the same dimensions as u , independent of the dimensions of the space Ω . The price to pay is the field u must be computed and stored separately since (56) for μ must be solved backward in time. Summarizing, the gradient of the objective function is now calculated via:

- (1) *Field estimation*: Obtain the current field u^n by solving

$$\partial_t u^n = b(u^n, \theta^n), \quad u^n(0) = u_0(\theta^n). \quad (60)$$

- (2) *Adjoint field estimation*: Obtain the adjoint field μ^n by solving

$$\partial_t \mu^n = -(\partial_u b(u^n, \theta^n))^T \mu^n, \quad \mu^n(T) = \lambda \partial_u f(u^n(T)). \quad (61)$$

- (3) *Gradient calculation*: Compute the gradient $(\nabla_{\theta} E)^n$ via

$$(\nabla_{\theta} E)^n = \nabla_{\theta} I(\theta^n) - (\nabla_{\theta} u_0(\theta^n))^T \mu^n(0) - \int_0^T (\partial_{\theta} b(u^n(t), \theta^n))^T \mu^n(t) dt. \quad (62)$$

Note that equations (60) for u and (61) for μ are adjoint in both space and time. As a result the numerical simulation of these equations has to be done with care, as the integration scheme used for one equation needs to be the adjoint of the other. This is preferably done by using schemes that are self-adjoint. For recent literature on the topic we refer the reader to [22, 43, 44].

3.2. Descent with pre-conditioning of the gradient. Once we have calculated the gradient of the objective function at θ^n , we can make a downhill step in the cost function landscape using

- (4) *Descent step with pre-conditioning*:

$$\theta^{n+1} = \theta^n - \alpha^n B^n (\nabla_{\theta} E)^n, \quad (63)$$

where B^n is a pre-conditioning $M \times M$ matrix (recall that $\theta \in \Omega \subseteq \mathbb{R}^M$), and $\alpha^n > 0$ is the step size that is tuned optimally at each iteration via line search: this can be done using classical merit functions as discussed in [45].

The estimate of the matrix B^n deserves some further comments. Ideally, B^n should be the inverse of the Hessian of the objective function $E(\theta^n)$, but this Hessian is typically difficult to calculate. Therefore, a simpler solution is to use the Hessian of the prior $I(\theta^n)$, which in the case of a Gaussian measure is simply the inverse covariance matrix C^{-1} (which is independent of θ). Since this estimate coincides with the Hessian of $E(\theta^n)$ only when $\lambda = 0$, it will deteriorate when λ increases and the pre-conditioning may become inefficient. If that is the case, it may be useful to switch to “quasi-Newton” methods such as the BFGS algorithm, or the Limited-Memory BFGS algorithm when M is very large (> 100). In the applications treated in this paper, the naive pre-conditioning depending only on the prior $I(\theta)$ turned out to be sufficient to perform the optimization efficiently.

Since we are typically interested in calculating (6) for a range of values of z , instead of fixing z and trying to determine the corresponding Lagrange multiplier λ in (51), it is easier to vary λ and determine *a posteriori* which value of z this leads to. Indeed this offers a parametric representation of $\theta^*(z)$ via

$$\theta^*(z(\lambda)) = \tilde{\theta}^*(\lambda), \quad z(\lambda) = f(u(T, \tilde{\theta}^*(\lambda))), \quad (64)$$

where $\tilde{\theta}^*(\lambda)$ is the minimizer of $E(\theta)$ at λ fixed. We can then also calculate $I(\theta^*(z(\lambda))) = I(\tilde{\theta}^*(\lambda))$ and estimate $P(z(\lambda)) \propto \exp(-I(\tilde{\theta}^*(\lambda)))$.

4. APPLICATIONS

4.1. Elasticity of an heterogeneous rod. In this section we study a model for a one-dimensional rod with random elasticity coefficient subject to a prescribed external mechanical forcing (i.e. pulling at one end). Even though this model (or generalizations thereof) may be of interest in actual applications (e.g. as a coarse-grained model of DNA stretching [8, 10, 30]), it is primarily used here as a simple illustrative example of the tools and concepts introduced in Secs. 2 and 3. In particular, we use LDT to locate the most likely configurations leading to extreme responses and we show that such realizations dominate the statistics asymptotically.

In the case of forcing increasing linearly in time, we are able to derive analytical results which are used to validate our numerical method. We also study the extreme events that occur under a nonlinear forcing, when no analytical solution is available.

4.1.1. Continuous model with random structure. Consider a one-dimensional elastic rod of length 1 that is being pulled at one end with a time-dependent force and whose energy is specified in terms of its displacement field $u : [0, 1] \rightarrow \mathbb{R}$ via

$$V(u, t) = \frac{1}{2} \int_0^1 \mathcal{D}(x) |\partial_x u|^2 dx - r(t) u(1), \quad (65)$$

where the first term is the total internal energy of the rod and the second term is the external energy (negative of the work potential); $\mathcal{D}(x) > 0$ is the elasticity coefficient, assumed to be spatially dependent, and $r(t)$ is a prescribed external forcing protocol acting on the right end of the rod – the specific form of $r(t)$ will be introduced later. The dynamics of the rod is governed by the Euler-Lagrange equation associated with (65):

$$\partial_t^2 u = \partial_x (\mathcal{D}(x) \partial_x u) \quad x \in (0, 1), \quad (66)$$

with initial conditions to be prescribed later and boundary conditions

$$u(t, 0) = 0, \quad \mathcal{D}(1) \partial_x u(t, 1) = r(t), \quad \forall t \geq 0. \quad (67)$$

In order to introduce uncertainty in the model we make the elasticity random, i.e. we take $\mathcal{D}(x) \equiv \mathcal{D}(x, \vartheta)$. Here we will assume that $\mathcal{D}(x, \vartheta)$ is piecewise constant over blocks of size $1/M$ for some $M \in \mathbb{N}$, with independent values in each block. Specifically, we take:

$$\mathcal{D}(x, \vartheta) = \sum_{k=1}^M \varphi_k(x) g(\vartheta_k), \quad (68)$$

where the functions $\{\varphi_k\}_{k=1}^M$ are given by

$$\varphi_k(x) = \begin{cases} 1 & \text{if } M^{-1}(k-1) \leq x < M^{-1}k \\ 0 & \text{otherwise} \end{cases}; \quad (69)$$

g is a given function; and $\{\vartheta_k\}_{k=1}^M$ are i.i.d. random variables. Below we will consider two cases:

Case 1. Here we assume that $g : (0, \infty) \rightarrow (0, \infty)$ with

$$g(u) = u^{-1} \quad (70)$$

and we take the variable $\{\vartheta_k\}_{k=1}^M$ to be exponentially distributed, i.e.

$$\mathbb{P}(\vartheta_k \geq \theta_k) = e^{-\alpha \theta_k}, \quad \theta_k \geq 0, \quad \alpha > 0. \quad (71)$$

This choice implies that

$$S(\eta) = \log \mathbb{E} e^{\langle \eta, \vartheta \rangle} = - \sum_{k=1}^M \log(1 - \alpha^{-1} \eta_k), \quad \eta_k < \alpha \quad \forall k = 1, \dots, M, \quad (72)$$

so that

$$I(\theta) = \sum_{k=1}^M (\alpha \theta_k - 1 - \log \theta_k) \quad \theta_k > 0 \quad \forall k = 1, \dots, M. \quad (73)$$

Case 2. Here we assume that $g : \mathbb{R} \rightarrow (0, \infty)$ with

$$g(u) = \frac{1}{2}u + \sqrt{\frac{1}{4}u^2 + 1}, \quad (74)$$

and we take the variable $\{\theta_k\}_{k=1}^M$ to be normally distributed with variance $\sigma^2 > 0$, i.e.

$$\theta_k = \mathcal{N}(0, \sigma^2) \quad (75)$$

This choice implies that

$$S(\eta) = \frac{1}{2} \sum_{k=1}^N \sigma^2 \eta_k^2, \quad I(\theta) = \frac{1}{2} \sum_{k=1}^N \sigma^{-2} \theta_k^2. \quad (76)$$

Given this random input, our aim is to investigate the statistics of the displacement of the right end of the rod at time T : this amounts to considering the observable $f(u(T)) = u(T, 1)$, and studying the behavior of

$$P(z) = \mathbb{P}(u(T, 1, \vartheta) \geq z) \quad \text{for } z \gg 1. \quad (77)$$

Below we will analyze the behavior of this quantity in two cases, when the forcing $r(t)$ in (65) is linear in t and when it is not – the first situation is amenable to analytical treatment whereas the second is not in general. Note that in both situations, the behavior of $P(z)$ for large z will depend on how fast $g(u)$ decays to zero: due to the shape of g this will depend on the right tail of the distribution of θ_k in Case 1 and on its left tail in Case 2.

4.1.2. *Discrete model.* To perform the numerics, we need to consider a spatially discretized version of the model above. We do so by introducing the discrete energy

$$V(u, t) = \frac{1}{2} \sum_{j=0}^{N-1} \mathcal{D}_{j+1}(\vartheta) \frac{(u_{j+1} - u_j)^2}{\Delta x} - r(t) u_N, \quad (78)$$

in which $u_j = u(j\Delta x)$, $\mathcal{D}_j = \mathcal{D}(j\Delta x)$, $\Delta x = 1/N$. Alternatively, (78) can be thought of as the energy for a system of $N+1$ beads u_j connected by N springs with random spring constants $\mathcal{D}_j(\vartheta)$. The dynamics obeys the system of ODEs

$$\partial_t^2 u_j = \frac{\mathcal{D}_{j+1}}{\Delta x^2} (u_{j+1} - u_j) - \frac{\mathcal{D}_j}{\Delta x^2} (u_j - u_{j-1}), \quad j = 1, \dots, N-1, \quad (79)$$

with fixed boundary condition $u_0 = 0$ at the left end and dynamic boundary condition

$$\partial_t^2 u_N = -\frac{\mathcal{D}_N}{\Delta x^2} (u_N - u_{N-1}) + \frac{r(t)}{\Delta x} \quad (80)$$

at the right end. We will pick $N = PM$ for some $P \in \mathbb{N}$, so that by our choice for $\mathcal{D}_j(\vartheta)$ in (68) we have

$$\mathcal{D}_j(\vartheta) = g(\theta_k) \quad \text{for } [j/P] = k, \quad j = 1, \dots, N, \quad k = 1, \dots, M. \quad (81)$$

Since we focus on the statistics of the observable $f(u(T)) = u_N(T) = u(T, 1)$ that measures the displacement at time T of the right end point with respect to its initial position, the cost function is

$$E(u, \theta) = I(\theta) - \lambda u_N(T), \quad (82)$$

to optimize on the parameters $\{\theta_k\}_{k=1}^M$. We will minimize (82) using the adjoint method to compute the gradient. As shown in the Appendix, the adjoint equations read

$$\partial_t^2 \mu_j = \frac{\mathcal{D}_{j+1}}{\Delta x^2} (\mu_{j+1} - \mu_j) - \frac{\mathcal{D}_j}{\Delta x^2} (\mu_j - \mu_{j-1}), \quad j = 1, \dots, N-1, \quad (83)$$

with conditions at the boundaries given by

$$\mu_0(t) = 0, \quad \partial_t^2 \mu_N = -\frac{\mathcal{D}_N}{\Delta x^2} (\mu_N - \mu_{N-1}), \quad (84)$$

and final conditions

$$\mu_j(T) = 0, \quad \partial_t \mu_j(T) = \lambda \delta_{j,N}. \quad (85)$$

The gradient of the cost function can be expressed as

$$\nabla_{\theta} E(u(\theta), \theta) = \nabla I(\theta) - G^T \nabla \mathcal{D}(\theta), \quad (86)$$

where $\nabla \mathcal{D}(\theta)$ is the $N \times M$ tensor with entries $\partial \mathcal{D}_j(\theta) / \partial \theta_k$, $j = 1, \dots, N$, $k = 1, \dots, M$, and G is a vector with entries

$$G_j = \int_0^T \frac{u_j - u_{j-1}}{\Delta x} \frac{\mu_j - \mu_{j-1}}{\Delta x} dt, \quad j = 1, \dots, N. \quad (87)$$

4.1.3. *Linear forcing.* Assume that $r(t) = at$ for some $a > 0$ and as initial conditions for (101) take

$$u(0, x) = 0, \quad \partial_t u(0, x) = a \int_0^x \frac{dx'}{\mathcal{D}(x', \theta)}, \quad \forall x \in [0, 1]. \quad (88)$$

The solution to (66) equipped with the boundary conditions in (67) is

$$u(t, x, \vartheta) = at \int_0^x \frac{dx'}{\mathcal{D}(x', \vartheta)}. \quad (89)$$

Let us consider the implications of this formula in *Case 1*, which is suitable to derive analytical results. Eq. (89) implies that

$$u(T, 1, \vartheta) = aT \int_0^1 \frac{dx'}{\mathcal{D}(x', \vartheta)} = \frac{aT}{M} \sum_{k=1}^M \vartheta_k, \quad (90)$$

where we used the specific form of $\mathcal{D}(x, \vartheta)$ given in (68) with g given in (70). Note that since the discrete equivalent to the initial conditions (102) is

$$u_j(0) = 0, \quad \partial_t u_j(0) = \frac{a}{M} \sum_{k=1}^j \vartheta_k, \quad (91)$$

the result (90) also holds for the discretized model, i.e. we have

$$u_N(T, \vartheta) = \frac{aT}{M} \sum_{k=1}^M \vartheta_k. \quad (92)$$

From (71), this implies that $u(T, 1, \vartheta) = u_N(T, \vartheta)$ follows a gamma distribution with shape parameter M and rate parameter $\alpha M(aT)^{-1}$:

$$\begin{aligned} P(z) &= \int_z^\infty \frac{(\alpha M(aT)^{-1})^M u^{M-1}}{(M-1)!} e^{-\alpha M(aT)^{-1}u} du \\ &= \frac{1}{(M-1)!} \Gamma(M, \alpha M(aT)^{-1}z), \end{aligned} \quad (93)$$

where $\Gamma(\cdot, \cdot)$ is the upper incomplete Gamma function. When $z \gg 1$ with M fixed, (93) gives

$$P(z) \sim \frac{(\alpha M(aT)^{-1}z)^{M-1}}{(M-1)!} e^{-\alpha M(aT)^{-1}z}, \quad (94)$$

meaning that

$$\log P(z) \sim -\alpha M(aT)^{-1}z + (M-1) \log(\alpha M(aT)^{-1}z) - \log(M-1)!. \quad (95)$$

In this last expression the second and third terms at the right hand side are subdominant over the first, $\alpha M(aT)^{-1}z$, and disappear in the limit as $z \rightarrow \infty$. It is useful to keep these terms for comparison with the result (36) in Theorem 1 and the result (39), which we do next.

If we solve

$$\min I(\theta) = \min \sum_{k=1}^M (\alpha \theta_k - 1 - \log \alpha \theta_k) \quad \text{subject to} \quad u(T, 1, \theta) = \frac{aT}{M} \sum_{k=1}^M \theta_k = z, \quad (96)$$

we get

$$\theta_k^*(z) = (aT)^{-1}z \quad \text{for } k = 1, \dots, M. \quad (97)$$

As a result

$$I(\theta^*(z)) = M(\alpha(aT)^{-1}z - 1 - \log(\alpha(aT)^{-1}z)), \quad (98)$$

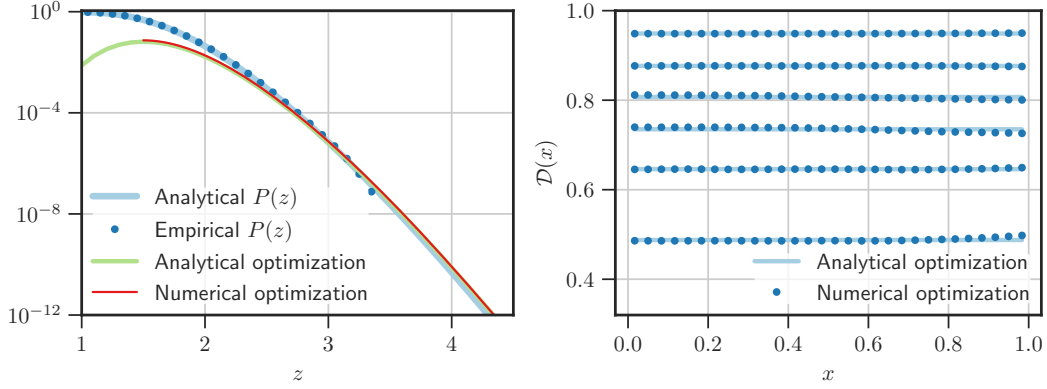


FIGURE 1. Linear forcing with $a = 0.1$, final time $T = 15$, initial conditions (91), and the statistical prior of *Case 1*. The numerics are performed with $M = N = 30$. Left panel: Comparison between the exact expression for $P(z)$ in (93), the empirical MC estimate with 2×10^7 samples, the analytical LDT estimate (98), and the LDT estimate obtained via numerical optimization. Right panel: Comparison between the analytical (97) and the numerical instantons, for $z = 1.58, 1.71, 1.85, 2.04, 2.32, 3.08$ from top to bottom.

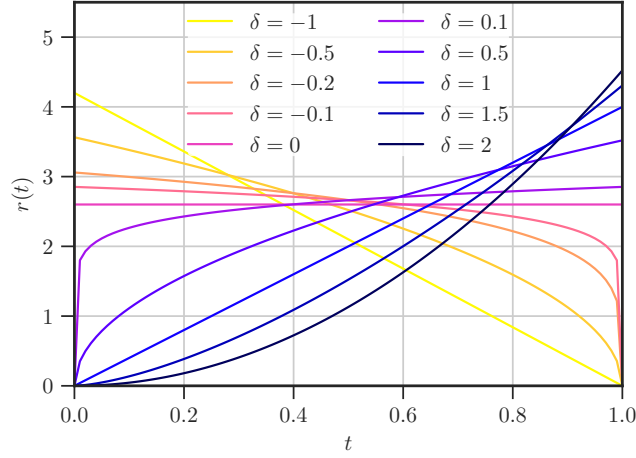


FIGURE 2. The forcing protocols $r_\delta(t)$ in (100), which are decreasing functions of t when $\delta < 0$ and increasing functions when $\delta > 0$.

which from (95) is consistent with $\log P(z) \sim -I(\theta^*(z))$ as $z \rightarrow \infty$, as predicted by (36). Note also that here

$$\eta_k^*(z) = \partial_{\theta_k} I(\theta^*(z)) = \alpha - aTz^{-1} \quad \text{for } k = 1, \dots, M. \quad (99)$$

Since this implies that $|\eta_k^*(z)| \rightarrow \alpha$ as $z \rightarrow \infty$, this means that the condition in (37) is not satisfied here.

In Fig. 1 we compare the asymptotic estimate (98) with the exact expression (93). We also check that the numerical optimization is consistent with the analytical one, which is important to validate the numerical code described below.

4.1.4. Nonlinear forcing. Next we consider nonlinear forcing protocols of the type

$$r(t) = at^\beta \quad \text{and} \quad r(t) = a(T-t)^\beta \quad \text{both with } a, \beta > 0. \quad (100)$$

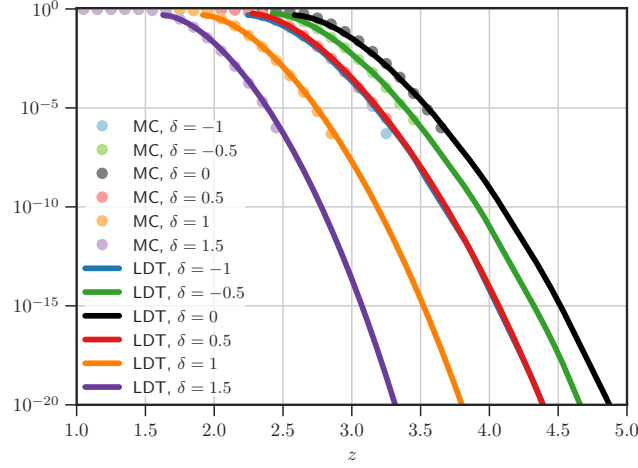


FIGURE 3. Comparison between the empirical distributions $P(z)$ obtained via MC sampling and their LDT estimate. The sampling works down to events whose probability is about the inverse of the MC sampling size, while the LDT optimization allows us to extend the tails to much smaller probabilities.

Letting $s = +1$ if $r(t) = at^\beta$ and $s = -1$ if $r(t) = a(T-t)^\beta$, we will use $r_\delta(t)$ with $\delta = s\beta$ as shorthand to describe the family of forcing protocols. They are shown in Fig. 2.

As initial conditions for (66) we take

$$u(0, x) = 0, \quad \partial_t u(0, x) = 0, \quad \forall x \in [0, 1]. \quad (101)$$

At discrete level these initial conditions read

$$u_j(0) = 0, \quad \partial_t u_j(0) = 0. \quad (102)$$

In this section we restrict ourselves to *Case 2* and we use $M = N = 30$ and final time $T = 1$. Observing that the mean elasticity $\mathbb{E}(\mathcal{D}(x)) = 1$ (as for *Case 1*), the average velocity of propagation of the waves along the bar is also 1. Thus, 1 is the average time that a signal takes to propagate from the right end to the left end. This means that taking $T = 1$ we are considering a short transient strongly out of equilibrium, where the random structure will contribute in a non-homogeneous way.

To integrate (79) and (80) numerically, we use a velocity-Verlet integrator, which is of second order, symplectic, and time reversible, with a time step of 10^{-3} . The optimization is performed as described in Sec. 3, using (86) and (87).

Let us now describe our results. In Fig. 3 the LDT estimates of $P(z)$ are compared to the empirical estimates obtained via MC with 2×10^6 samples, showing good agreement. Next we look at the specific elasticity structure of the optimizers, $\mathcal{D}(x, \theta^*(z))$. These are shown in Fig. 4. As can be seen, the region that is relevant for having an extreme extension $u(T = 1, 1)$ occupies only the right half of the space domain, independent of the protocol. This makes sense since on average the signal takes a time 1 to cross the whole domain: For a point x_0 to influence $u(T = 1, 1)$ the signal needs to have time to propagate to $x = 1$. As a result, the points on the left side will not have the possibility to influence the dynamics at all, and the optimal state of $\mathcal{D}(x, \theta)$ is determined by mere minimization of $I(\theta)$ with no dynamical constraint. In contrast, on the right side of the domain, $\mathcal{D}(x, \theta)$ must take low values to allow for large values of $u(T = 1, 1)$ – since these low values are unlikely, this also accounts for the drop in probability observed in Fig. 3. Fig. 4 also indicates that $\mathcal{D}(x, \theta^*(z))$ depends on the forcing protocol. This dependency can again be interpreted intuitively by realizing that the region that impacts $u(T, 1)$ the most will be the one that is reached

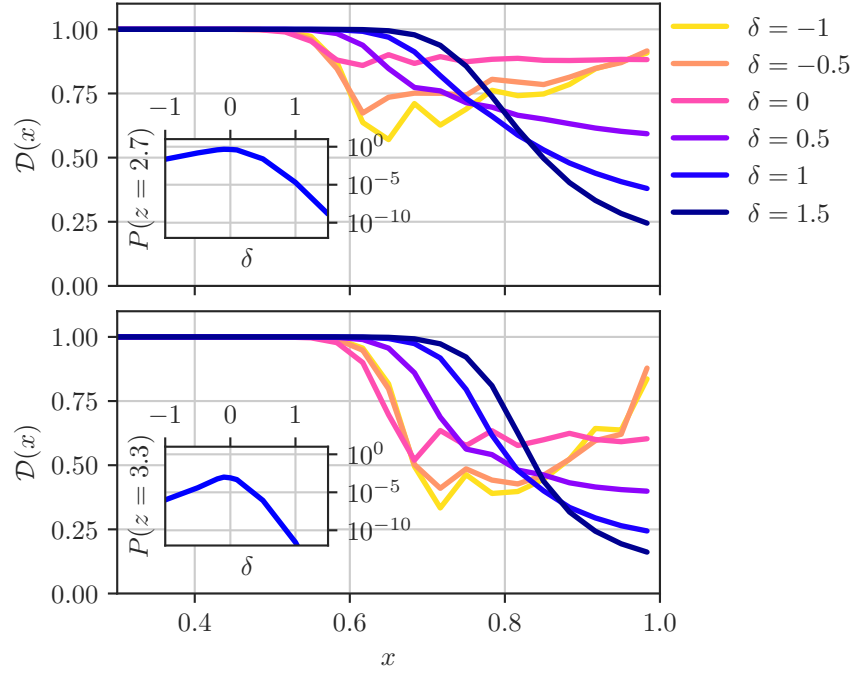


FIGURE 4. Top panel: Elasticity structure of the instantons for $z \geq 2.7$, for the different protocols labeled by δ . Inset: the probability $P(z = 2.7)$ as a function of the forcing protocol. Bottom panel: Same as in the top panel, but for $z \geq 3.3$. Inset: the probability $P(z = 3.3)$ as a function of δ in the forcing protocol.

by a strong signal (i.e. the propagation front of the most intense part of the forcing) and is able to send a strong feedback back to the right end at final time – this feedback is what is accounted for by the backward evolution of the adjoint equation in the optimization. So, the earlier the most intense part of the forcing takes place, the further from the right end a low elasticity peak appears. This explains why going towards negative δ the low-elasticity peak moves to the left in Fig. 4, and the constant forcing ($\delta = 0$) is the one where the low elasticity contribution is the most uniformly distributed.

Note that in this framework it is possible to compare how likely the protocols are to produce extreme realizations of a given size, as shown in the insets in Fig. 4. In this sense, the constant protocol appears to be the optimal one. This is consistent with the fact that $\delta = 0$ is the highest curve in Fig. 3.

To further clarify the role of the instantons and why they dominate the dynamics and the statistics of the extreme events, it is useful to “filter” the conditional events such that $u(T, 1) \geq z$ in the following way: First, we fix a size z and generate via MC a large set of θ such that $u(T, 1, \theta) \geq z$. Second, we average over such conditional set to obtain the mean conditional event and its fluctuations around the mean, which is generally very close to the instanton $\theta^*(z)$. Third, we decompose the fluctuations $\theta - \theta^*(z)$ into the components parallel and perpendicular to $\eta^*(z)$, i.e. the normal to the hypersurface $\Omega(z)$. This procedure is then repeated for various z .

In Fig. 5 we show the outcome of this analysis for the protocol with $\delta = 1.5$ and for two different values of z – analogous results hold for the other kinds of forcing as well. As can be seen the average event $u(T, 1) \geq z$ lies on top of the instanton $\theta^*(z)$, with fluctuations independent of the size of the event and also of the position along the rod (upper panels). The decomposition shows that the components perpendicular to $\eta^*(z)$ are independent of the size of the event, and

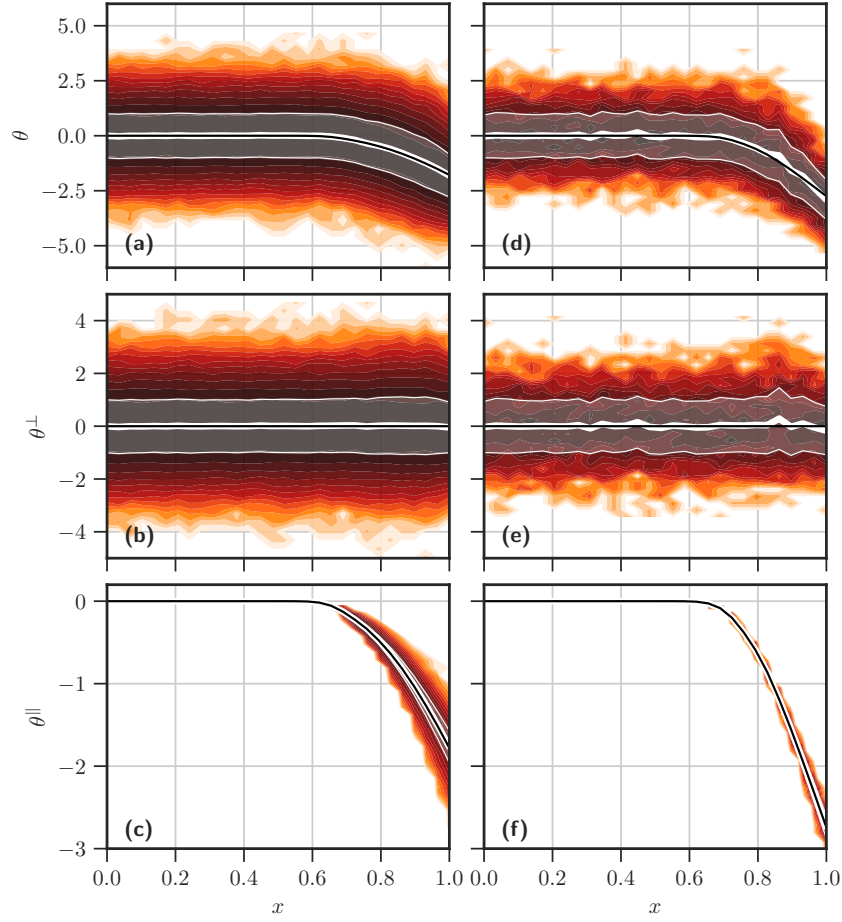


FIGURE 5. Comparison between the instanton $\theta^*(z)$ (black solid line) and the Monte Carlo sampling on the distribution of ϑ , conditioned on $u_N(1) = u(1, 1) \geq z$ (color map with intensity proportional to the empirical probability density; thick white line = mean; thin white lines = 1 standard deviation range around the mean). Left panels: $z = 2.10$, right panels: $z = 2.40$. The top panels show the full data: the instanton agrees with the mean, but the variance does not substantially change going to more extreme events. The two central panels show the fluctuations perpendicular to $\eta^*(z)$, confirming that their amplitude is independent of the size of the event (left and right panels have the same variance) and homogeneous in space. The bottom panels show the fluctuations in the direction parallel to $\eta^*(z)$, indicating that their amplitude decreases as z increases, as predicted by the theory in Sec. 2.

basically independent of the dynamics too. Their mean and standard deviation are the mean and the standard deviation of the unconstrained random variables ϑ (central panels). In contrast, the parallel fluctuations are small and tend to zero as z increases (bottom panels). The scaling of the fluctuations is analyzed in more detail in Fig. 6, which shows that they are $O(1)$ in the direction perpendicular to $\eta^*(z)$ and $O(|\eta^*(z)|^{-1})$ in the direction parallel to it, consistent with the theoretical predictions.

4.2. Extreme events in optical turbulence.

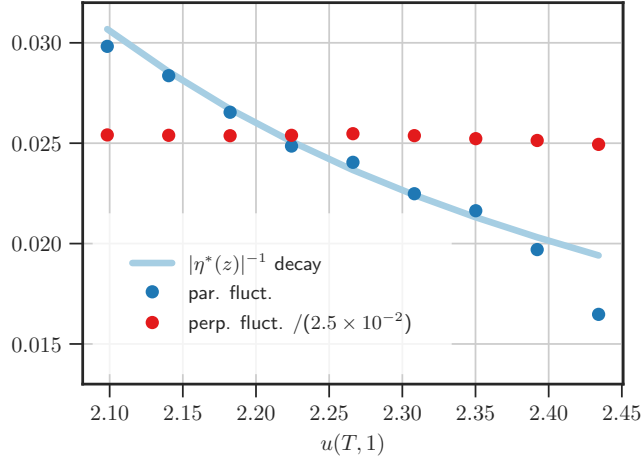


FIGURE 6. Increasing z , the fluctuations in the direction perpendicular to $\eta^*(z)$ stay constant, whereas in the parallel direction they scale as $O(|\eta^*(z)|^{-1})$. Both behaviors are predicted analytically and here confirmed numerically.

4.2.1. The 1D NLSE and the LDT formalism. The nonlinear Schrödinger equation (NLSE) in one dimension arises in a variety of different contexts such as surface gravity waves [32, 46], nonlinear fiber optics [2], plasmas [3] and Bose-Einstein condensates [21, 33]. Here we will focus on applications of NLSE in nonlinear optics, a domain that has seen exciting experimental developments in recent years [28, 37, 39]. Specifically, we study the problem of the onset of rogue waves out of a bath of random waves taken as initial condition for NLSE, which is a key question in *integrable turbulence* [1, 11, 17, 36, 47].

In non-dimensional units, the 1D NLSE for the envelope of a light beam propagating in an optical fiber reads

$$\partial_\xi \Psi = i \frac{1}{2} \Psi_{\tau\tau} + i |\Psi|^2 \Psi, \quad \tau \in \Gamma, \quad (103)$$

where $\Gamma = [0, T]$, with periodic boundary conditions $\Psi(\xi, 0) = \Psi(\xi, T)$, and a suitable initial condition $\Psi(0, \tau) = \Psi_0(\tau)$, at the input end of the fiber $\xi = 0$. The non-dimensional distance ξ , time τ , and envelope Ψ are related to the respective physical quantities x , t , and ψ via characteristic constants that depend on the specifics of the optical fiber: $x = \mathcal{L}_0 \xi$, $t = \mathcal{T}_0 \tau$ and $\psi = \sqrt{\mathcal{P}_0} \Psi$. For instance, if we pick $\mathcal{T}_0 = 5$ ps, $\mathcal{L}_0 = 0.5$ km, $\mathcal{P}_0 = 0.5$ mW, the NLSE (103) models an optical fiber with dispersion $|\beta_2| = \mathcal{T}_0^2 / \mathcal{L}_0 = 50$ ps²km⁻¹ and nonlinearity $\gamma = 1 / (\mathcal{L}_0 \mathcal{P}_0) = 4$ km⁻¹mW⁻¹.

Let us denote by $\{\hat{\Psi}_n\}_{n \in \mathbb{Z}}$ the Fourier component of $\{\Psi(\tau)\}_{\tau \in [0, T]}$, i.e.

$$\hat{\Psi}_n = \frac{1}{T} \int_0^T e^{-i\omega_n \tau} \Psi(\tau) d\tau, \quad \Psi(\tau) = \sum_{n=-\infty}^{+\infty} e^{i\omega_n \tau} \hat{\Psi}_n, \quad (104)$$

where $\omega_n = 2\pi n/T$ and $n \in \mathbb{Z}$. Equation (103) is derived under the *quasi-monochromatic* assumption, meaning that the spectrum \hat{C}_n defined as

$$\hat{C}_n = \frac{1}{T} \int_0^T e^{-i\omega_n \tau} C(\tau) d\tau, \quad C(\tau - \tau') = \mathbb{E}(\Psi_0(\tau) \bar{\Psi}_0(\tau')), \quad (105)$$

must be narrow – here and below the bar denoting complex conjugation. We will consider a Gaussian spectrum with

$$\hat{C}_n = \mathcal{A} e^{-\omega_n^2 / (2\Delta)} \quad \mathcal{A} > 0, \quad \Delta > 0, \quad -M \leq n \leq M, \quad M > 0, \quad (106)$$

and $\hat{C}_n = 0$ for $|n| > M$. Assuming that the initial $\Psi(0, \tau)$ is a Gaussian field with mean zero and covariance $C(\tau - \tau')$, this implies the representation

$$\Psi(0, \tau, \vartheta) = \sum_{n=-M}^M e^{i\omega_n \tau} \hat{C}_n^{1/2} \vartheta_n, \quad (107)$$

where ϑ_n are complex Gaussian variables with mean zero and covariance $\mathbb{E} \vartheta_n \bar{\vartheta}_m = \delta_{m,n}$, $\mathbb{E} \vartheta_n \vartheta_m = \mathbb{E} \bar{\vartheta}_n \bar{\vartheta}_m = 0$. Note that the spectral amplitude is related to the optical power $P(\xi, \tau) = |\psi(\xi, \tau)|^2$ (statistically homogeneous in τ) via $\mathcal{A} = \mathbb{E}(P) / \sum_n e^{-\omega_n^2 / (2\Delta)}$. The initial statistical state of the system is thus completely determined given the two parameters Δ and $\mathbb{E}(P)$, and the average power $\mathbb{E}(P)$ is relevant to optical experiments – it also enjoys the property of being invariant under the NLSE evolution in the variable ξ , i.e. it can be measured at the input or at the output of the optical fiber, equivalently.

In the set-up above, we will investigate extreme fluctuations of the optical power at the output of the optical fiber ($\xi = L$). Recalling that $|\Psi(L, \tau)| = \sqrt{P(L, \tau)}$, this amounts to looking at the statistics of

$$f(\Psi(\vartheta)) = \max_{\tau \in \Gamma} |\Psi(L, \tau, \vartheta)|, \quad L > 0. \quad (108)$$

Analyzing this observable using the framework developed in Secs. 2 and 3 amounts to minimizing the cost function (this is (49))

$$E(\Psi, \theta) = I(\theta) - \lambda f(\Psi) \quad \text{with} \quad I(\theta) = \frac{1}{2} \sum_{n=-M}^M |\theta_n|^2. \quad (109)$$

This minimization must be performed on the $2 \times (2M + 1)$ -dimensional space $\Omega \subseteq \mathbb{C}^{2M+1}$ of the initial conditions. The gradient of the cost function (109) is given by

$$\nabla_\theta E(\Psi(\theta), \theta) = \nabla_\theta I(\theta) + \Re(J(L, \tau_*))^T \frac{\Re(\Psi(L, \tau_*))}{|\Psi(L, \tau_*)|} + \Im(J(L, \tau_*))^T \frac{\Im(\Psi(L, \tau_*))}{|\Psi(L, \tau_*)|}, \quad (110)$$

where $\Psi(L, \tau_*) \equiv \max_{\tau \in \Gamma} |\Psi(L, \tau)|$. The field Ψ is evolved with (103) and the initial condition depends on the point $\theta \in \Omega$ through the mapping $\Psi(0, \theta)$ defined in (107), with the difference that here θ is no longer random. The matrix J (also complex) evolves according to

$$\partial_\xi J(\xi, \tau) = \int_0^L d\xi' \left(\frac{\delta b(\Psi(\xi))}{\delta \Psi(\xi')} J(\xi', \tau) + \frac{\delta b(\Psi(\xi))}{\delta \bar{\Psi}(\xi')} \bar{J}(\xi', \tau) \right), \quad (111)$$

where $b(\Psi(\xi))$ is a shorthand for the right hand side of (103): explicitly

$$\int_0^L d\xi' \frac{\delta b(\xi)}{\delta \Psi(\xi')} J(\xi') = \left(\frac{i}{2} \partial_{\tau\tau} + 2i |\Psi(\xi)|^2 \right) J(\xi), \quad (112)$$

$$\int_0^L d\xi' \frac{\delta b(\xi)}{\delta \bar{\Psi}(\xi')} \bar{J}(\xi') = i (\Psi(\xi))^2 J(\xi). \quad (113)$$

The initial condition for (111) is

$$J(\xi = 0, \theta) = \nabla_\theta \Psi(0, \theta). \quad (114)$$

Before turning to the results, let us explain how the numerical simulations were performed. Equations (103) and (111) were evolved from $\xi = 0$ to $\xi = L$ (up to $L = 0.2$) using the pseudo-spectral second order Runge-Kutta exponential-time-differencing method (ETDRK2) [12, 27] with step $d\xi = 5 \times 10^{-4}$ on a periodic box $[0, T]$ discretized by 2^{12} equidistant grid points. The size $T = 30$ is found large enough for the boundary conditions to not affect the statistics on the spatio-temporal scales considered. Each Monte Carlo simulation involves 10^6 realizations of the random initial data constructed via (107), with $M = 45$. Adding more modes to the initial condition does not affect the results in any significant way. The minimization was performed in the space Ω (with high dimension $2 \times (2M + 1) = 182$). This step was carried out via steepest descent with adaptive step (line search) and preconditioning of the gradient, using the covariance of the initial condition as metric, as explained in Sec. 3.

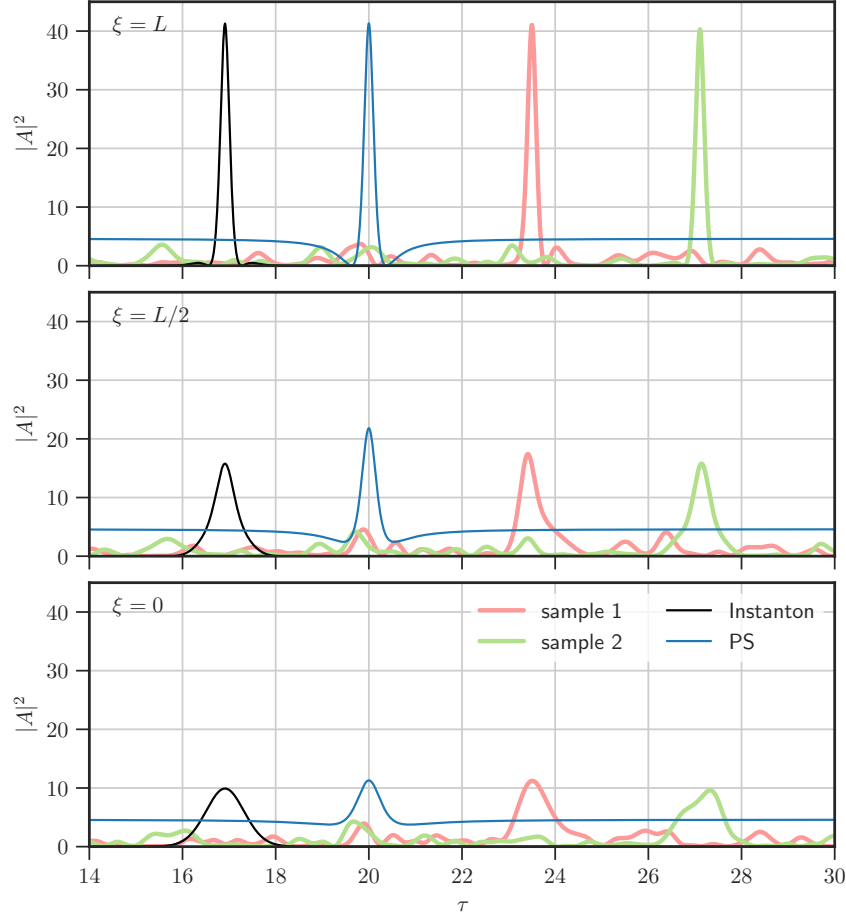


FIGURE 7. Set 1: The paths of occurrence of two extreme events plotted are compared with the instanton and the Peregrine solution reaching the same maximum power at $\xi = L$. Shown is the quantity $|A(\xi, \tau)|^2$, i.e. the power in units of average power, at three different locations ($L = 0.2$). The solution are shifted away from one another for clarity, exploiting homogeneity in τ .

4.2.2. Results. For generality, we present the results for the normalized field $A(\xi, \tau) = \Psi(\xi, \tau) / \sqrt{\mathbb{E}(P)}$ using non-dimensional units. One can easily obtain the physical dimensions by applying the straightforward transformations given below equation (103). Four sets of parameters have been chosen to explore different regimes: In Set 1, we take $\Delta = \pi$, $\mathbb{E}(P) = 5/4$; in Set 2, $\Delta = \pi/2$, $\mathbb{E}(P) = 5/4$; in Set 3, $\Delta = 3\pi/2$, $\mathbb{E}(P) = 5/4$; and in Set 4, $\Delta = \pi$, $\mathbb{E}(P) = 5/9$.

There have been recent claims, supported by both numerical and experimental evidence [37, 39], about the universality of the Peregrine Soliton (PS) as a pathway to optical rogue waves out of a random background. For this reason, we carried out a comparison between the instantons and the PS. In Fig. 7, the path of occurrence of two extreme events is shown for Set 1, selected among the events in the random sampling with maximum power amplification $|A|^2 = P/\mathbb{E}(P)$ exceeding a value of 40. The instanton and the PS reaching the same power amplification are also plotted.

In Fig. 8 the probability $P(z) = \mathbb{P}(\max_{\tau} |A(L, \tau)| \geq z)$ is shown for various values of L , showing good agreement between the results from MC sampling and those from LDT optimization. A rough estimate for the onset threshold of optical rogue waves is $|A|_{RW} = 4\sqrt{2/\pi\mathbb{E}(|A|)} \approx 2.8$ [16],

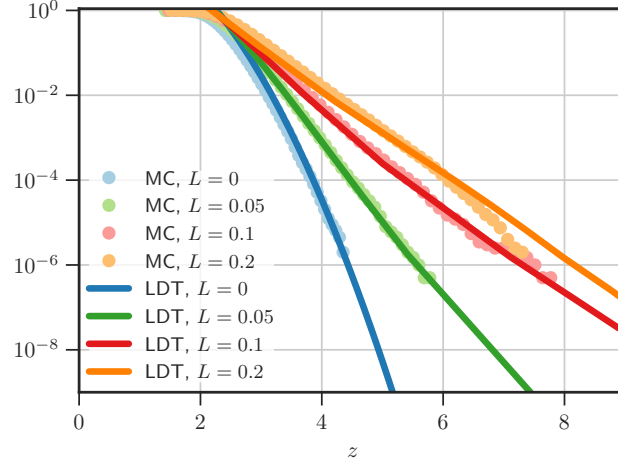


FIGURE 8. Set 1: Comparison between the probability distributions of $\max_{\tau} |A(L, \tau)|$ in the periodic time window $[0, T]$ obtained by MC with 10^6 samples, and their corresponding LDT estimates computed using the optimization method. The plot captures the tail fattening due to the NLSE dynamics, as the output point is taken at increasing distance L from the input. The rogue-wave threshold is $|A|_{RW} \approx 2.8$. The characteristic length of emergence of the coherent structures is $L_c = 0.2$, compatible with the observed tail fattening.

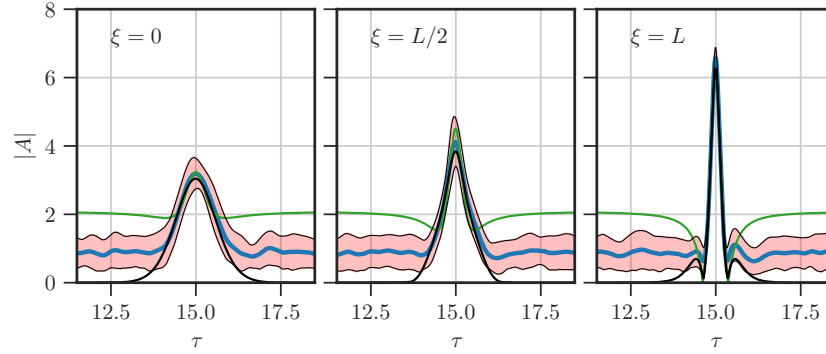


FIGURE 9. Set 1: Results of the conditioning on the sampling for $\max_{\tau \in \Gamma} |A(L, \tau)| \geq z = 6.25$, with $L = 0.2$. Shown is the average of the conditional event (blue line), surrounded by the 1 std range (red area). The instanton (black line) is the optimal event reaching maximal intensity $A = z$ at the output point $\xi = L$. The PS is also represented (green line), normalized to have intensity z at the point of maximal space-time focusing. From left to right, the panels are at $\xi = 0$, $\xi = L/2$ and $\xi = L$.

independently of the set considered because of the use of the normalized variable A . As can be seen, the focusing NLSE increases the probability of large excursions of $|A(L, \tau)|$ compared to its initial Gaussian value with expectation $\mathbb{E}(|A(L=0, \tau)|) = \sqrt{\pi/4}$. This happens gradually as the distance L separating the input from the output increases. The tail fattening can be interpreted quantitatively in terms of the typical lengths of the coherent structures of NLSE. Defining the linear length as $L_{\text{lin}} = 2/\Delta^2$ and the nonlinear length as $L_{\text{nl}} = 1/\mathbb{E}(P)$, the typical length of

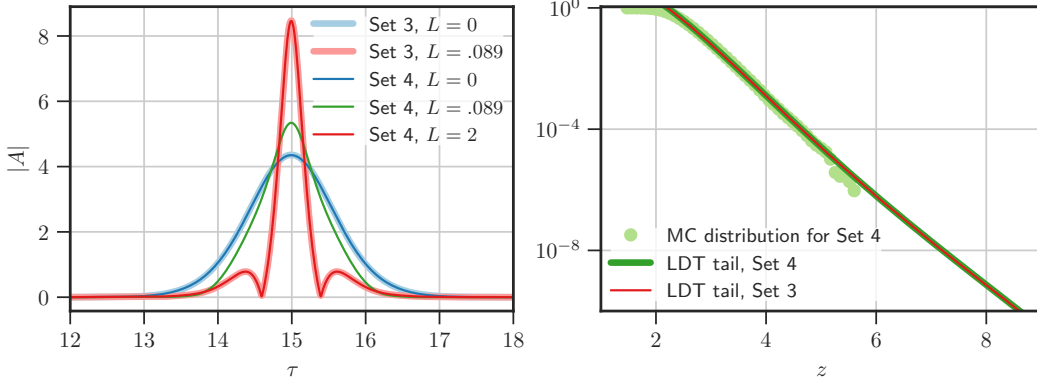


FIGURE 10. The two panels show how knowledge of the LDT tail at the output point L for a given Δ and $\mathbb{E}(P)$ allows us to recover the LDT tail for an arbitrary Δ' , with the properly rescaled mean power $\mathbb{E}(P)'$, space L' , and time τ' . Left: Instanton reaching $\max_{\tau \in \Gamma} |A(L, \tau)| = 8.5$, for sets 3 and 4. Right: $\mathbb{P}(\max_{\tau} |A(L, \tau)| \geq z)$ from MC sampling and tail estimate for Sets 3 and 4, at an equivalent rescaled output point L . Note that not only the probability tail is the same for the two sets, but also the entire distribution, as the scale invariance establishes a complete equivalence between two sets having the same value of the ratio $\sqrt{\mathbb{E}(P)}/\Delta$.

emergence of a coherent structure starting from a small hump is $L_c = \frac{1}{2}\sqrt{L_{\text{lin}}L_{\text{nonlin}}}$. This gives $L_c = 0.2$ for Set 1, in good agreement with the width of the spatial transient over which the fast tail fattening takes place.

The asymptotic agreement of the probabilities shown in Fig. 8 is a numerical evidence that the focusing NLSE (103) with random initial data (107) satisfies an LDP. Additional support for the LDP is found in Fig. 9, where we compare the instanton with the sampling mean. Looking at the signal to noise ratio, one sees that the events reaching a certain extreme amplification are all very similar. According to the results in Sec. 2, these events are expected to have typical fluctuations in the direction perpendicular to the instanton in the space Ω : notice how away from the focusing region (determined by the direction perpendicular to the instanton because there the instanton is vanishing) the observable $|A|$ fluctuates with standard deviation $\sqrt{\mathbb{E}(P)}/2\sqrt{(4-\pi)/2}/\sqrt{\mathbb{E}(P)} \simeq 0.57$ around the expected value $\sqrt{\pi/2}\sqrt{\mathbb{E}(P)}/2/\sqrt{\mathbb{E}(P)} \simeq 0.89$, exactly as expected for typical events. Instead, the extreme size of the event is due to the component parallel to the instanton in Ω , with small fluctuations in this direction: As a matter of fact, in the focusing region (determined by the component parallel to the instanton) the signal to noise ratio becomes very big, meaning that, as z increases, the extreme rogue waves with $\max_{\tau} |A(\tau, L)| \geq z$ become closer to the instanton reaching $\max_{\tau} |A(\tau, L)| = z$.

Interestingly, from the knowledge of the LDT tails for a particular configuration of the parameters Δ and $\mathbb{E}(P)$ we can derive the LDT tails for any combination of Δ and $\mathbb{E}(P)$, using only analytical transformations. This is possible thanks to two properties: First, the scale invariance of the NLSE; second, the way the parameter $\mathbb{E}(P)$ appears in the cost function (109). Indeed the term $I(\theta)$ is independent of $\mathbb{E}(P)$, and from (107) the term $f(\Psi(\theta))$ can be seen as a function of $\sqrt{\mathbb{E}(P)}\theta$.

- Starting from the second property, we have that given a fixed spectral width Δ and a mean power $\mathbb{E}(P)$, giving the cost function (109) $E(\theta, \lambda)$, the cost function $E'(\theta, \lambda)$ associated to a new

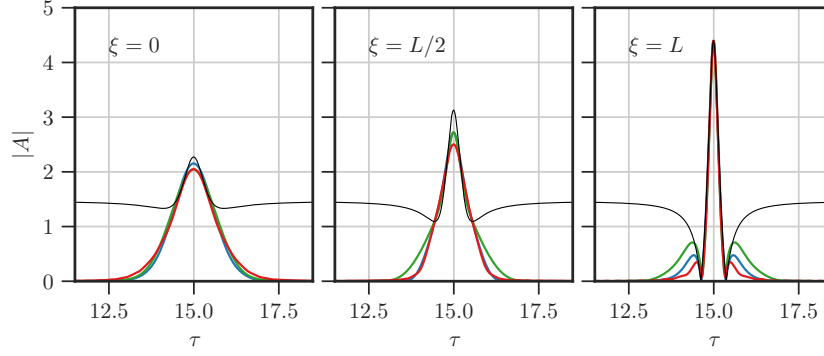


FIGURE 11. Snapshots at increasing spatial coordinate from left to right ($\xi = 0$, $\xi = 0.1$, $\xi = 0.2$) of instantons reaching the same peak intensity, for the three sets of parameters with different spectral width: Set 1 ($\Delta = \pi$) in red; Set 2 ($\Delta = \pi/2$) in green; and Set 3 ($\Delta = 3\pi/2$) in blue. The PS reaching the same final height (at the point of maximal focusing) is also plotted in black. For all the profiles, striking agreement is observed around the point of maximal focusing in space-time, while significant differences are observed away from that point.

mean power $\mathbb{E}(P)'$ (but same spectral width) can be written as

$$E'(\theta, \lambda) = \frac{\mathbb{E}(P)}{\mathbb{E}(P)'} E(\theta', \lambda'), \quad \theta' = \theta \sqrt{\frac{\mathbb{E}(P)'}{\mathbb{E}(P)}}, \quad \lambda' = \lambda \frac{\mathbb{E}(P)'}{\mathbb{E}(P)}. \quad (115)$$

Since λ' is nothing but a rescaling of λ , and they are both arbitrary variables, E and E' represent actually the same landscape, just differing by a positive factor and a rescaling of the variables. This implies that if we know an instanton $\theta^*(z)$ and its associated probability $P(z)$ for the mean power $\mathbb{E}(P)$, we also know that for mean power $\mathbb{E}(P)'$ the same event will have instanton $\theta'^*(z) = \theta^*(z) \sqrt{\mathbb{E}(P)'/\mathbb{E}(P)}$ with associated probability

$$P'(z) = P(z) \frac{\mathbb{E}(P)}{\mathbb{E}(P)'}. \quad (116)$$

Thus, keeping Δ fixed, the LDT tails for a given $\mathbb{E}(P)$ are sufficient to generate the LDT tails for any mean power $\mathbb{E}(P)'$, using (116).

- Using the scale invariance of the NLSE, it is possible to make a similar argument to extend the LDT tails to arbitrary Δ . Knowing that initial conditions with the same ratio $\sqrt{\mathbb{E}(P)}/\Delta$ are scale invariant for the NLSE, one can pick an arbitrary spectral width Δ' . This gives a new mean power $\mathbb{E}(P)' = \mathbb{E}(P)(\Delta'/\Delta)^2$, and allows us to compute the new length $L' = (\Delta/\Delta')^2 L$ and time coordinate $\tau' = (\Delta/\Delta')\tau$. Thus, a bijection is established between the two parameter sets, where each pair is characterized by the same non-dimensional instanton and same probability. Hence, knowing the LDT tails at different L for one value of the spectral width, one is able to obtain the whole spatial transient of the LDT tails for an arbitrary spectral width. In Fig. 11 the invariance of the non-dimensional instanton and of the LDT tail is shown for Sets 3 and 4, which yield the same dynamics once the appropriate rescaling is performed.

Figs. 7 and 9 confirm that the high-power pulses arising spontaneously from a random background tend to the shape of the PS around its maximum space-time concentration [39]. Interpreting this in light of the gradient-catastrophe regularization [4], it is clear that such characteristic shape of the extreme power amplifications is independent of the solitonic content of the field, although it is shared with the local behavior of an exact solitonic solution. The random extreme realizations quickly diverge from the PS away from the maximum, however. In contrast, the instantons characterize all the essential dynamics of the extreme events in integrable turbulence.

They give an approximation of the extreme excursions that is much more accurate than the PS, as can be observed in Fig. 9, and their shape adapts to the size of the event. In addition, unlike the PS, they come with probabilistic information and allows the estimation of the distribution tail, as seen in Fig. 8, with mathematical justification in the LDT result (36). Furthermore, the instantons depend on the statistical state of the random background, as shown in Fig. 11, while the PS is always the same. Because of these properties and their connection with the gradient catastrophe (which is their generating mechanism), the instantons can be important objects for further investigations in integrable turbulence. In this context, recent results [13] suggest that the formation of extreme coherent structures may not necessarily be linked to integrability, but may pertain to a more general class of systems with instabilities (e.g. due to non-resonant interactions) leading to spatio-temporal concentration phenomena.

5. CONCLUSIONS

We have shown that tools and concepts from large deviation theory (LDT), combined with optimization tools from optimal control, can be used to analyze rare events in the context of dynamical systems subject to random input in their parameters and/or their initial conditions. In our examples, the predictions from LDT were actually valid in a wide region of parameter space. This means that the large deviation regime is attained for events that are rare but still quite frequent, and extend down to extremely low probabilities, exploring regions unattainable through brute-force MC sampling. In addition, the instantons provide us with information about the mechanism of the events that can only be extracted from MC sampling via non-trivial filtering. Under this light, the LDT method stands as a competitive alternative, or at least a useful complement, to brute-force MC.

ACKNOWLEDGMENT

We thank Georg Stadler for useful comments regarding the optimization method, and Gilles Francfort for suggesting the elastic rod application. We are also grateful to Lamberto Rondoni, Themis Sapsis, Freddy Bouchet, Hugo Touchette and Pierre Suret for interesting discussions.

APPENDIX A. CALCULATIONS OF SECTION 4.1

Using the convention that $\mathcal{D}_{N+1} = 0$, the evolution equation (79) can be rewritten as a system of first order ODEs,

$$\begin{cases} \partial_t u_j = p_j \\ \partial_t p_j = \frac{\mathcal{D}_{j+1}}{\Delta x^2} (u_{j+1} - u_j) - \frac{\mathcal{D}_j}{\Delta x^2} (u_j - u_{j-1}) + \delta_{j,N} \frac{r(t)}{\Delta x} \end{cases}, \quad j = 1, \dots, N \quad (117)$$

with fixed boundary condition in the origin,

$$u_0(t) = 0, \quad (118)$$

and initial conditions

$$u_j(0) = 0, \quad p_j(0) = 0. \quad (119)$$

To make the notation compact, we will use:

$$X = \begin{pmatrix} u \\ p \end{pmatrix}, \quad Y = \begin{pmatrix} \eta \\ \mu \end{pmatrix}, \quad (120)$$

column vectors in \mathbb{R}^{2N} . Then, (117) can be written as

$$\partial_t X = b(X, \theta), \quad (121)$$

where $b(X, \theta)$ is the $2N$ -dimensional vector with the components of the RHS of (117). Note that (121) is in the general form (50) (linear system of ODEs), and this is helpful to make direct contact with the formulas (56) and (59), and thereby compute the gradient of the cost function (82) as

$$\nabla_{\theta} E = \nabla_{\theta} I(\theta) - \int_0^T (\partial_{\theta} b)^T Y dt, \quad (122)$$

with Y the adjoint field to X . Let us start by deriving the adjoint equation. One can easily check that the linearization of the operator $b(X, \theta)$ for small variations of X reads

$$\partial_X b(\theta) = \begin{pmatrix} 0 & \text{Id} \\ B(\theta) & 0 \end{pmatrix}, \quad (123)$$

with $B_{jk} = \frac{\mathcal{D}_{j+1}}{\Delta x^2} (\delta_{j+1,k} - \delta_{j,k}) - \frac{\mathcal{D}_j}{\Delta x^2} (\delta_{j,k} - \delta_{j-1,k})$.

Id is the $N \times N$ identity matrix and we recall that $\mathcal{D}_j = \mathcal{D}(\theta_j)$, by (74). It is the adjoint operator $(\partial_X b)^T$ that we need to compute, defined implicitly by the identity

$$\langle (\partial_X b)^T Y, X' \rangle_{\mathbb{R}^{2N}} = \langle Y, \partial_X b X' \rangle_{\mathbb{R}^{2N}}, \quad (124)$$

where $\langle \cdot, \cdot \rangle_{\mathbb{R}^{2N}}$ denotes the standard scalar product in \mathbb{R}^{2N} . Using (124) we obtain,

$$\begin{aligned} \langle Y, \partial_X b X' \rangle_{\mathbb{R}^{2N}} &= \sum_{j=1}^N \left(\eta_j p'_j + \mu_j \left(\frac{\mathcal{D}_{j+1}}{\Delta x^2} (u'_{j+1} - u'_j) - \frac{\mathcal{D}_j}{\Delta x^2} (u'_j - u'_{j-1}) \right) \right) \\ &= \sum_{j=1}^N \left(\eta_j p'_j + \left(\frac{\mathcal{D}_{j+1}}{\Delta x^2} (\mu_{j+1} - \mu_j) - \frac{\mathcal{D}_j}{\Delta x^2} (\mu_j - \mu_{j-1}) \right) u'_j \right), \end{aligned} \quad (125)$$

where in the last passage we just reorganized the indices in the sum in an equivalent way, provided that we assume the boundary condition

$$\mu_0(t) = 0. \quad (126)$$

Comparing the last line of (125) with the LHS of (124), we deduce that

$$(\partial_X b)^T = \begin{pmatrix} 0 & B(\theta) \\ \text{Id} & 0 \end{pmatrix} \quad (127)$$

which is the transpose of the RHS of (123) ($B(\theta)$ is symmetric), as we should expect. Though, starting from the identity (124) is the rigorous way to obtain the adjoint operator, making the proper boundary conditions arise naturally. Plugging the result (127) into (56), we finally obtain the adjoint equation

$$\begin{cases} \partial_t \eta_j = \frac{\mathcal{D}_{j+1}}{\Delta x^2} (\mu_{j+1} - \mu_j) - \frac{\mathcal{D}_j}{\Delta x^2} (\mu_j - \mu_{j-1}), & j = 1, \dots, N, \\ \partial_t \mu_j = \eta_j \end{cases} \quad (128)$$

with boundary condition (126). To obtain the correct conditions at final time, it is sufficient to observe that the final conditions of (56) now read

$$\eta_j(T) = \lambda \partial_{u_j} f(u(T)) = \lambda \delta_{j,N}, \quad \mu_j(T) = 0. \quad (129)$$

Let us now compute $(\partial_{\theta} b)^T$, again starting from the definition of the adjoint operator:

$$\langle (\partial_{\theta} b)^T Y, w \rangle_{\mathbb{R}^N} = \langle Y, \partial_{\theta} b w \rangle_{\mathbb{R}^{2N}}, \quad (130)$$

where $w \in \mathbb{R}^N$ and

$$\begin{aligned} (\partial_{\theta} b) &= \begin{pmatrix} 0 \\ \nabla_{\theta} B(\theta) \end{pmatrix} \quad (\text{two } N \times N \text{ blocks}) \\ (\nabla_{\theta} B)_{jk} &= \frac{\mathcal{D}'(\theta_{j+1})}{\Delta x^2} (u_{j+1} - u_j) \delta_{j+1,k} - \frac{\mathcal{D}'(\theta_j)}{\Delta x^2} (u_j - u_{j-1}) \delta_{j,k}. \end{aligned} \quad (131)$$

With the convention that $\mathcal{D}'(\theta_{N+1} = 0)$, a straightforward calculation yields

$$\begin{aligned} \langle Y, \partial_\theta b w \rangle_{\mathbb{R}^{2N}} &= \sum_{j=1}^N \mu_j \left(\frac{\mathcal{D}'(\theta_{j+1})}{\Delta x^2} (u_{j+1} - u_j) w_{j+1} - \frac{\mathcal{D}'(\theta_j)}{\Delta x^2} (u_j - u_{j-1}) w_j \right) \\ &= \sum_{j=1}^N \left(\frac{\mathcal{D}'(\theta_j)}{\Delta x^2} (u_j - u_{j-1}) (\mu_j - \mu_{j-1}) \right) w_j, \end{aligned} \quad (132)$$

from which, comparing with the LHS of (130), we observe that

$$((\partial_\theta b)^T Y)_j = \mathcal{D}'(\theta_j) \frac{u_j - u_{j-1}}{\Delta x} \frac{\mu_j - \mu_{j-1}}{\Delta x}. \quad (133)$$

Now, integrating in time according to (122),

$$\int_0^T ((\partial_\theta b)^T Y)_j dt = \mathcal{D}'(\theta_j) \int_0^T \frac{u_j - u_{j-1}}{\Delta x} \frac{\mu_j - \mu_{j-1}}{\Delta x} dt, \quad (134)$$

leads to (86).

REFERENCES

- [1] D. S. Agafontsev and V. E. Zakharov. Integrable turbulence and formation of rogue waves. *Nonlinearity*, 28(8):2791, 2015.
- [2] N. Akhmediev, J. M. Dudley, D. R. Solli, and S. K. Turitsyn. Recent progress in investigating optical rogue waves. *Journal of Optics*, 15(6):060201, 2013.
- [3] H. Bailung, S. K. Sharma, and Y. Nakamura. Observation of Peregrine solitons in a multicomponent plasma with negative ions. *Physical Review Letters*, 107(25):255005, 2011.
- [4] M. Bertola and A. Tovbis. Universality for the focusing nonlinear Schrödinger equation at the gradient catastrophe point: rational breathers and poles of the tritronquée solution to Painlevé I. *Communications on Pure and Applied Mathematics*, 66(5):678–752, 2013.
- [5] A. A. Borovkov and B. A. Rogozin. On the multi-dimensional central limit theorem. *Theory of Probability & its Applications*, 10(1):55–62, 1965.
- [6] A. Borzi and V. Schulz. *Computational optimization of systems governed by partial differential equations*. Computational Science & Engineering. SIAM, 2011.
- [7] M. Broniatowski and A. Fuchs. Tauberian theorems, Chernoff inequality, and the tail behavior of finite convolutions of distribution functions. *Advances in Mathematics*, 116(1):12–33, 1995.
- [8] C. Bustamante, J. E. Marko, E. D. Siggia, and S. Smith. Entropic elasticity of lambda-phage DNA. *Science*, 265(5178):1599–1599, 1994.
- [9] F. Cérou and A. Guyader. Adaptive multilevel splitting for rare event analysis. *Stochastic Analysis and Applications*, 25(2):417–443, 2007.
- [10] P. Cluzel, A. Lebrun, C. Heller, R. Lavery, J.-L. Viovy, D. Chatenay, and F. Caron. DNA: an extensible molecule. *Science*, 271(5250):792–794, 1996.
- [11] W. Cousins and T. P. Sapsis. Reduced-order precursors of rare events in unidirectional nonlinear water waves. *J. Fluid Mech.*, 790:368–388, 2016.
- [12] S. M. Cox and P. C. Matthews. Exponential time differencing for stiff systems. *Journal of Computational Physics*, 176(2):430–455, 2002.
- [13] G. Dematteis, T. Grafke, and E. Vanden-Eijnden. Rogue waves and large deviations in deep sea. *Proceedings of the National Academy of Sciences*, page 201710670, 2018.
- [14] A. Dembo and O. Zeitouni. *Large deviations techniques and applications. Corrected reprint of the second edition*. Stochastic Modelling and Applied Probability, 38. Springer-Verlag, Berlin, 2010.
- [15] U. Einmahl and J. Kuelbs. Dominating points and large deviations for random vectors. *Probab. Theory Related Fields*, 105(4):529–543, Dec. 1996.
- [16] R. El Koussaifi, A. Tikan, A. Toffoli, S. Randoux, P. Suret, and M. Onorato. Spontaneous emergence of rogue waves in partially coherent waves: a quantitative experimental comparison between hydrodynamics and optics. *Physical Review E*, 97(1):012208, 2018.
- [17] M. Farazmand and T. P. Sapsis. A variational approach to probing extreme events in turbulent dynamical systems. *arXiv preprint arXiv:1704.04116*, 2017.
- [18] U. Frisch and D. Sornette. Extreme deviations and applications. *Journal de Physique I*, 7(9):1155–1171, 1997.
- [19] C. Giardinà, J. Kurchan, V. Lecomte, and J. Tailleur. Simulating rare events in dynamical processes. *Journal of statistical physics*, 145(4):787–811, 2011.
- [20] P. Glasserman, P. Heidelberger, P. Shahabuddin, and T. Zajic. Multilevel splitting for estimating rare event probabilities. *Operations Research*, 47(4):585–600, 1999.

- [21] E. P. Gross. Structure of a quantized vortex in boson systems. Nuovo Cimento, 20(454), 1961.
- [22] W. W. Hager. Runge-Kutta methods in optimal control and the transformed adjoint system. Numerische Mathematik, 87(2):247–282, 2000.
- [23] M. Ittis. Sharp asymptotics of large deviations in \mathbb{R}^d . Journal of Theoretical Probability, 8(3):501–522, 1995.
- [24] M. Ittis. Sharp asymptotics of large deviations for general state-space Markov-additive chains in \mathbb{R}^d . Statistics & Probability Letters, 47(4):365–380, 2000.
- [25] J. L. Jensen. Saddlepoint approximations. Oxford Statistical Science Series, 16. Oxford University Press, New York, 1995.
- [26] S. Juneja and P. Shahabuddin. Rare-event simulation techniques: an introduction and recent advances. Handbooks in operations research and management science, 13:291–350, 2006.
- [27] A.-K. Kassam and L. N. Trefethen. Fourth-order time-stepping for stiff PDEs. SIAM Journal of Scientific Computing, 26(4):1214–1233, 2005.
- [28] B. Kibler, J. Fatome, C. Finot, G. Millot, F. Dias, G. Genty, N. Akhmediev, and J. M. Dudley. The Peregrine soliton in nonlinear fibre optics. Nature Physics, 6(10):790, 2010.
- [29] J. Kuelbs. Large deviation probabilities and dominating points for open convex sets: nonlogarithmic behavior. Annals of probability, pages 1259–1279, 2000.
- [30] F. Lankaš, J. Šponer, P. Hobza, and J. Langowski. Sequence-dependent elastic properties of DNA. Journal of Molecular Biology, 299(3):695–709, 2000.
- [31] P. Ney. Dominating points and the asymptotics of large deviations for random walk on \mathbb{R}^d . The Annals of Probability, 11(1):158–167, 1983.
- [32] M. Onorato, S. Residori, U. Bortolozzo, A. Montina, and F. Arecchi. Rogue waves and their generating mechanisms in different physical contexts. Physics Reports, 528(2):47–89, 2013.
- [33] L. P. Pitaevsky. Vortex lines in an imperfect Bose gas. Soviet Physics - Journal of Experimental and Theoretical Physics, 13(451), 1961.
- [34] R.-E. Plessix. A review of the adjoint-state method for computing the gradient of a functional with geophysical applications. Geophysical Journal International, 167(2):495–503, 2006.
- [35] F. Ragone, J. Wouters, and F. Bouchet. Computation of extreme heat waves in climate models using a large deviation algorithm. Proceedings of the National Academy of Sciences, page 201712645, 2017.
- [36] S. Randoux, P. Walczak, M. Onorato, and P. Suret. Intermittency in integrable turbulence. Physical Review Letters, 113(11):113902, 2014.
- [37] P. Suret, R. El Koussaifi, A. Tikan, C. Evain, S. Randoux, C. Szwaj, and S. Bielawski. Single-shot observation of optical rogue waves in integrable turbulence using time microscopy. Nature Communications, 7, 2016.
- [38] J. Tailleur and J. Kurchan. Probing rare physical trajectories with Lyapunov weighted dynamics. Nature Physics, 3(3):203, 2007.
- [39] A. Tikan, C. Billet, G. El, A. Tovbis, M. Bertola, T. Sylvestre, F. Gustave, S. Randoux, G. Genty, P. Suret, et al. Universality of the Peregrine soliton in the focusing dynamics of the cubic nonlinear Schrödinger equation. Physical Review Letters, 119(3):033901, 2017.
- [40] F. Tröltzsch. Optimal control of partial differential equations. Graduate Studies in Mathematics, 112. American Mathematical Soc., 2010.
- [41] E. Vanden-Eijnden and J. Weare. Rare Event Simulation of Small Noise Diffusions. Communications on Pure and Applied Mathematics, 65(12):1770–1803, Sept. 2012.
- [42] S. R. S. Varadhan. Large deviations. Courant Lecture Notes, 27. American Mathematical Soc., 2016.
- [43] A. Walther. Automatic differentiation of explicit Runge-Kutta methods for optimal control. Computational Optimization and Applications, 36(1):83–108, 2007.
- [44] L. C. Wilcox, G. Stadler, T. Bui-Thanh, and O. Ghattas. Discretely exact derivatives for hyperbolic PDE-constrained optimization problems discretized by the discontinuous Galerkin method. Journal of Scientific Computing, 63(1):138–162, 2015.
- [45] S. Wright and J. Nocedal. Numerical optimization. Springer Series in Operations Research. Springer, 2000.
- [46] V. E. Zakharov. Stability of periodic waves of finite amplitude on the surface of a deep fluid. Journal of Applied Mechanics and Technical Physics, 9(2):190–194, 1968.
- [47] V. E. Zakharov. Turbulence in integrable systems. Studies in Applied Mathematics, 122(3):219–234, 2009.

DIPARTIMENTO DI SCIENZE MATEMATICHE, POLITECNICO DI TORINO, CORSO DUCA DEGLI ABRUZZI 24, I-10129 TORINO, ITALY

MATHEMATICS INSTITUTE, UNIVERSITY OF WARWICK, COVENTRY CV4 7AL, UNITED KINGDOM

COURANT INSTITUTE, NEW YORK UNIVERSITY, 251 MERCER STREET, NEW YORK, NY 10012, USA